Flux-Profile Relationships in the Atmospheric Surface Layer

J. A. BUSINGER,[1] J. C. WYNGAARD,[2] Y. IZUMI[2] AND E. F. BRADLEY[3]

(Manuscript received 27 July 1970)

ABSTRACT

Wind and temperature profiles for a wide range of stability conditions have been analyzed in the context of Monin-Obukhov similarity theory. Direct measurements of heat and momentum fluxes enabled determination of the Obukhov length L, a key independent variable in the steady-state, horizontally homogeneous, atmospheric surface layer. The free constants in several interpolation formulas can be adjusted to give excellent fits to the wind and temperature gradient data. The behavior of the gradients under neutral conditions is unusual, however, and indicates that von Kármán's constant is ~0.35, rather than 0.40 as usually assumed, and that the ratio of eddy diffusivities for heat and momentum at neutrality is ~1.35, compared to the often-suggested value of 1.0. The gradient Richardson number, computed from the profiles, and the Obukhov stability parameter z/L, computed from the measured fluxes, are found to be related approximately linearly under unstable conditions. For stable conditions the Richardson number approaches a limit of ~0.21 as stability increases. A comparison between profile-derived and measured fluxes shows good agreement over the entire stability range of the observations.

1. Introduction

The importance of turbulent exchange processes in the atmospheric boundary layer to the general circulation of the atmosphere has long been recognized. Over a dry, flat, horizontally homogeneous land surface, the predominant processes are the vertical transport of momentum and sensible heat. A central and recurring feature of much of micrometeorological research has been to establish means of deriving these fluxes from wind speed and temperature profiles. Indeed, the literature abounds with profile formulas intended to accomplish this, particularly for the surface layer, the lowest 50 m or so of the boundary layer where the Coriolis force can be ignored and the fluxes can be assumed constant with height. Recent profile formulas reflect the similarity concepts put forward originally by Obukhov (1946). The first experimental evidence for these concepts was given by Monin and Obukhov (1954).

The testing of similarity predictions and profile formulas is ideally done with directly measured fluxes as well as profiles, a requirement which is rarely satisfied in micrometeorological field experiments. In the Kerang and Hay expeditions, for example, the results of which have been presented by Swinbank (1964) and Swinbank and Dyer (1968), and which have been extensively analyzed in the literature by Charnock (1967), Dyer (1965, 1967, 1968) and Swinbank (1968), stress was not measured directly but was inferred from the profiles.

The purpose of this paper is to present an analysis of a set of data that includes both profile and flux measurements over horizontally uniform, flat terrain. The results have been analyzed in dimensionless form, using the dimensionless quantities:

$$\mathrm{Ri}=\frac{g\partial\bar{\theta}/\partial z}{\bar{\theta}(\partial\bar{U}/\partial z)^2} \qquad \text{Richardson number, a stability parameter} \qquad (1)$$

$$\phi_m=\frac{kz}{u_*}\frac{\partial\bar{U}}{\partial z} \qquad \text{A dimensionless wind shear} \qquad (2)$$

$$\phi_h=\frac{z}{\theta_*}\frac{\partial\bar{\theta}}{\partial z} \qquad \text{A dimensionless temperature gradient} \qquad (3)$$

$$\alpha=\frac{K_h}{K_m}=\frac{\overline{w'\theta'}}{\overline{u'w'}}\frac{\partial\bar{U}/\partial z}{\partial\bar{\theta}/\partial z} \qquad \text{Ratio of the eddy transfer coefficients} \qquad (4)$$

$$\zeta=\frac{z}{L}=-\frac{kg\overline{w'\theta'}z}{\bar{\theta}u_*^3} \qquad \text{A dimensionless height} \qquad (5)$$

List of Symbols

g acceleration due to gravity
k von Kármán's constant
u, v, w longitudinal, lateral and vertical components of the wind
$\bar{S}$ mean horizontal wind speed $[(u^2+v^2)^{\frac{1}{2}}]$
$\bar{U}$ magnitude of the mean horizontal wind vector
z vertical coordinate
z_0 roughness length
θ potential temperature

[1] Work performed at Air Force Cambridge Research Laboratories on a National Research Council Associateship on leave from the University of Washington, Seattle.
[2] Air Force Cambridge Research Laboratories, Bedford, Mass.
[3] Commonwealth Scientific and Industrial Research Organization, Canberra, Australia.

u_* friction velocity $[(\tau_0/\rho)^{\frac{1}{2}}]$
θ_* scaling temperature $[-\overline{w'\theta'}/(ku_*)]$
L Obukhov length $[-\bar{\theta}u_*^3/(kg\overline{w'\theta'})]$
c_p specific heat of air at constant pressure
ρ air density
τ_0 surface shearing stress

An overbar denotes a time average and a prime the deviation from the average.

2. Instruments and experimental procedures

The data were obtained during the summer of 1968 at a site located in wheat-farming country of southwestern Kansas. A description of the site, the instruments, and the experimental procedures followed has already appeared in the literature (Haugen *et al.*, 1971). Only a brief outline will be given here.

Instruments were mounted on a 32 m tower located in the center of a one mile square field of wheat stubble ~18 cm tall. The neighboring section was also covered by wheat stubble, giving 2400 m of uniform fetch. There was no change in the surface during the experiments. Profile analyses to determine relevant characteristics of the surface included data from two masts of small cup anemometers (Bradley, 1969) with units mounted on each mast at heights of 23, 36, 50, 70 and 100 cm. These analyses suggest a surface roughnes length of ~2.4 cm and a zero plane displacement of ~10 cm.

Wind speeds on the 32 m tower were measured with three-cup anemometers manufactured by Control Equipment Corporation, mounted at heights of 2, 4, 5.66, 8, 11.3, 16, 22.6 and 32 m. In addition, two of these anemometers were mounted at 0.5 and 1 m, displaced ~30 m upwind from the tower. Temperature differences were measured with a high-resolution system developed by Stevens (1967), with sensors at 0.5, 1, 2, 4, 8, 16, 22.6 and 32 m. The instrument outputs were sampled once a second and stored on magnetic tape by a computer-controlled data acquisition system (Kaimal *et al.*, 1966).

Fluctuating wind components were measured with three-component sonic anemometers (Kaijo Denki, Model PAT 311) at 5.66, 11.3 and 22.6 m. Temperature fluctuations at the same levels were obtained with platinum wire resistance thermometers (Cambridge Systems Inc., Model 127). Surface stress was measured with two independent drag plates of the type described by Bradley (1968). These instruments were sampled 20 times per second and filtered, the former with a 10-Hz low-pass filter and the drag plates with a 5-Hz low-pass filter.

3. Data analysis

a. Data set

In all, 34 runs have been analyzed. The basic averaging period used was 15 min, an averaging period chosen rather for experimental convenience than for objective consideration of steady-state periods. A typical run length was one hour, occasionally shortened to 30 or 45 min during the actual experiment or during subsequent analyses. Twenty-eight of the runs to be discussed here were one hour long, two were 45 min, and four were 30 min. However, unless otherwise noted, the results to be presented will be based on the basic 15-min averaged data.

b. Determination of mean gradients

Gradients of mean wind speed were found by differentiating second-order polynomials in $\ln(z)$ fitted to speeds measured near the level in question. In most cases, five levels were used for each gradient computation: the level itself, two above, and two below. An 8 m wind shear, for example, was found from the 4, 5.66, 8, 11.3 and 16 m wind speeds. At 22.6 m, three speeds below and one above the level were used. The same method was used to compute temperature gradients, except at 5.66 and 11.3 m, where only four levels were used, two above and two below.

Computer experiments were performed to test this technique. The Businger-Dyer formulas, which will later be shown to fit the observations well, were used to generate sample unstable wind and temperature profiles, so that the gradients were known exactly. The gradients calculated by the curve-fit method agreed well with the exact values, the deviations being at most 2%. Under stable conditions the observed profiles are closely log-linear, as will be shown later. To test the method using the second-order polynomial in $\ln(z)$, the gradients were recalculated from the raw data by using as the polynomial, $a+b\ln(z)=cz$, which fits log-linear profiles exactly. Here the discrepancies were somewhat larger, but neither the zero intercepts nor the slopes of the dimensionless gradients differed significantly between the two methods. It was therefore concluded that the technique was satisfactory, and the gradients calculated at 4, 5.66, 8, 11.3, 16 and 22.6 m were taken as the basic set of profile data to be considered.

Temperature bath calibrations and on-site atmospheric comparisons indicate that the raw temperature data are accurate to ± 0.02C or better, independent of the ambient temperature. The accuracy of the wind speed data, however, is more difficult to assess because the response of a cup anemometer to a fluctuating horizontal wind field is nonlinear. Typical cup anemometers also respond nonlinearly to the vertical wind component. These characteristics lead to overspeeding, or indicated wind speeds greater than the actual horizontal wind speed. The importance of assessing overspeeding has been stressed by a few authors (e.g., Frenzen, 1966; MacCready, 1966) but quantitative estimates are rare.

For the data at hand, a good estimate of overspeeding can be made by comparing the cup anemometer speeds with the mean horizontal wind speeds from the sonic

anemometers at the corresponding levels. Sonic anemometers are ideal for this purpose, being absolute instruments, inherently linear (in contrast to most other wind speed instruments), and very accurate. Wind tunnel calibration and side-by-side atmospheric comparison tests (Kaimal and Haugen, 1969; Izumi and Barad, 1970) indicate that their mean wind speed readings are accurate to within 1%. Izumi and Barad made the speed comparison, and found that the cup speeds are ~10% too high for all stabilities. Therefore, the calculated wind shears were reduced by 10%. The residual overspeeding error resulting from applying a constant correction factor is of the order of ±3%.

It has become traditional in micrometeorological profile research to treat the mean horizontal wind speed, $\bar{S}$, rather than the magnitude of the mean horizontal wind vector, $\bar{U}$, although it could be argued that $\bar{U}$ is more appropriate. They are related, to a second-order approximation, by

$$\bar{S}=\bar{U}\left(1+\frac{\overline{v'^2}}{2\bar{U}^2}\right), \tag{6}$$

where $\overline{v'^2}$ is the variance of the lateral wind speed fluctuations. In principle, the $\bar{S}$ values can be converted to $\bar{U}$ values with Eq. (6); the correction is a weak function of height and stability and ranges from 1 to ~4% in the extreme. We have not made this correction, but have elected to work with wind speed in the manner of other investigators. Our point is simply that the wind shears used in the analysis are perhaps very slightly overestimated.

c. Determination of the surface shearing stress and heat flux

A detailed discussion of both the stress and heat flux measurements has been given by Haugen *et al.* (1971). These quantities were computed for each 15-min period, as were the profile data. In addition, 1-hr averages of the Reynolds stress and heat flux were computed for the three tower levels. The average of the four 15-min results for each run was compared with the hourly average to determine the contribution from low-frequency fluctuations to the fluxes. Individual runs yielded differences of about 5% in the extreme, with the overall difference for the entire data set being less than 1%. We therefore conclude that the 15-min averages provide adequate estimates of the Reynolds stress and heat flux for the purposes of this paper.

The results from the flux study of Haugen *et al.* which are used here will be briefly summarized. Both heat flux and Reynolds stress were found to be constant with height, within the limits of observational accuracy, although, overall, the sonic anemometer measurements indicated a decrease in stress between 5.66 and 22.6 m of about 6%. This is consistent with the decrease with height which would be expected from consideration of typical mean horizontal pressure gradients.

The trend was extrapolated linearly to the surface to obtain an estimate of overall surface stress, which was found to be lower, by a factor of 0.67, than the overall drag plate value. The discrepancy was ascribed to the subjective technique required to match the drag plate sample tray to its surroundings. No such uncertainty of exposure exists in the case of the sonic anemometer, so the overall sonic stresses were taken as a reference, and the factor 0.67 used as a correction factor for the drag plate measurements.

Although the drag plates did not measure accurately the absolute value of the stress, its temporal variation was considerably less than that of the eddy-correlation technique. Haugen *et al.* took advantage of this fact to reduce the scatter in data diagrams involving u_*. The comparison of their value of 1.3 for $\sigma(w)/u_*$ at neutrality with that of other workers is a useful justification of the stress correction procedure, particularly since it does not involve von Kármán's constant. The significance of this will become apparent in the next section.

We find, also, that the drag plate measurements lead to very closely ordered data diagrams, after correction for the overestimate, and are therefore the values used in this paper. The heat flux value for each run is the average of the measurements at the three sonic levels.

4. Results

a. Dimensionless wind shear, $\phi_m(\zeta)$

In Fig. 1, the dimensionless wind shear is plotted against ζ. The most remarkable aspect of this plot is that $\phi_m(0)$, the value at neutral stability, is about 1.15 (see inset in Fig. 1) rather than 1.0 as required. If the data are correct, we must conclude that von Kármán's constant k is not 0.40 as assumed, but is ~0.35. It is perhaps worth noting that the latter value agrees well with a recent prediction of 0.34 by Tennekes (1968).

The reduced value of k comes as a surprise, and it might be well to review the steps leading to its determination. The basic data set incorporates correction factors for both the wind shear and surface stress. While we feel that these factors are nearly completely effective, they are necessarily based on a limited data sample and are subject to some uncertainty. However, had the wind shear values not been corrected for overspeeding, the derived k would have been even smaller at 0.32. If the sonic anemometer stress values had been used to derive u_*, k would have been 0.34. It therefore appears unlikely that these factors could account for the departure from the usually assumed value of 0.40. As have most workers, we have assumed horizontal homogeneity, on the basis of visual observations of surface conditions and fetch; the lack of quantitative evidence of homogeneity introduces some uncertainty in the interpretations, but again it does not seem likely that this could account for the reduced k. Accordingly, we have used $k=0.35$ in the calculations in this paper, and

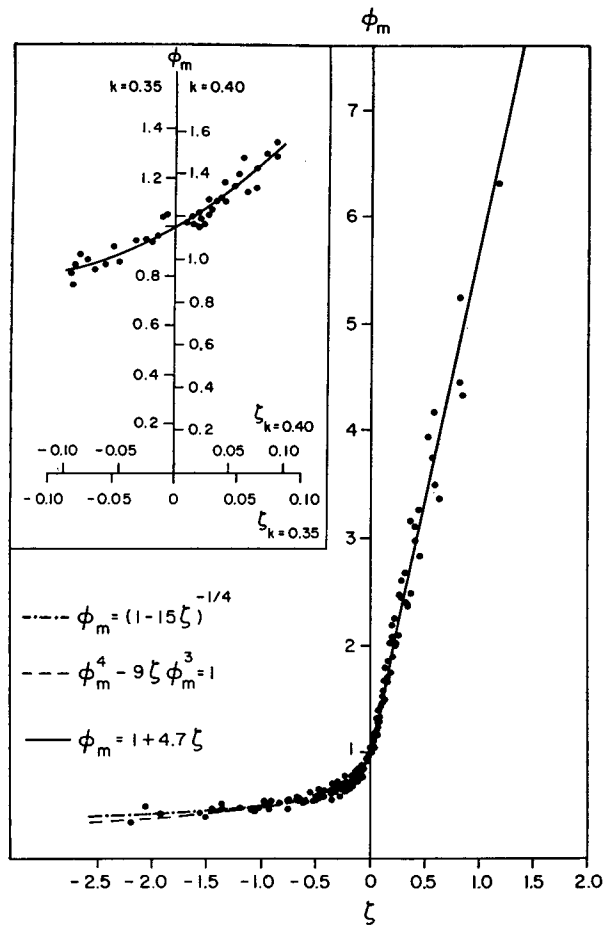

FIG. 1. Comparison of dimensionless wind shear observations with interpolation formulas.

look for further carefully performed experiments to verify this new value.

Several expressions for ϕ_m have been suggested, and the present data can be used to test them. A comprehensive survey will not be attempted here, but two formulas will be treated briefly; these are the so-called KEYPS formula (see Panofsky, 1963; Lumley and Panofsky, 1964), defined by

$$\phi_m{}^4-\gamma_1\zeta\phi_m{}^3=1, \tag{7}$$

and a modification of the KEYPS formula suggested by Businger (1966) and Dyer (unpublished), i.e.,

$$\phi_m=(1-\gamma_2\zeta)^{-\frac{1}{4}}. \tag{8}$$

These expressions are intended for unstable conditions, and have been chosen from the many described in the literature because of their relative simplicity. Each equation contains an adjustable constant. The free constants were determined by fitting Eqs. (7) and (8) to all the unstable observations and minimizing the mean square error, with the result that $\gamma_1=9$ and $\gamma_2=15$. Fig. 1 shows that both of these expressions fit the observations well.

One aspect of similarity theory that has been discussed extensively in the literature is the behavior of ϕ_m near neutral stability, $\zeta=0$. A quadratic curve fitted through the points shown in the inset in Fig. 1 has the form

$$\phi_m=1+3.0\zeta+10.2\zeta^2, \tag{9}$$

which has a slope of 3.0 at $\zeta=0$. Previous estimates of the slope vary widely, from 0.5 to near 5, reflecting the lack of agreement in the literature on the shape of ϕ_m. In both the KEYPS and Businger-Dyer formulas the slope at the origin is $\gamma/4$. Our values for the free constants then give slopes of 2.25 and 3.75, respectively, which deviate equally on either side of the measured value.

Under stable conditions, Fig. 1 indicates that ϕ_m varies essentially linearly with ζ over the entire stability range of the observations. The curve drawn has the form

$$\phi_m=1+4.7\zeta, \tag{10}$$

and the scatter of the data appears to allow slopes in the range 4.5–5.0. Eq. (10) is a good overall fit, but its slope near neutrality is about 50% greater than indi-

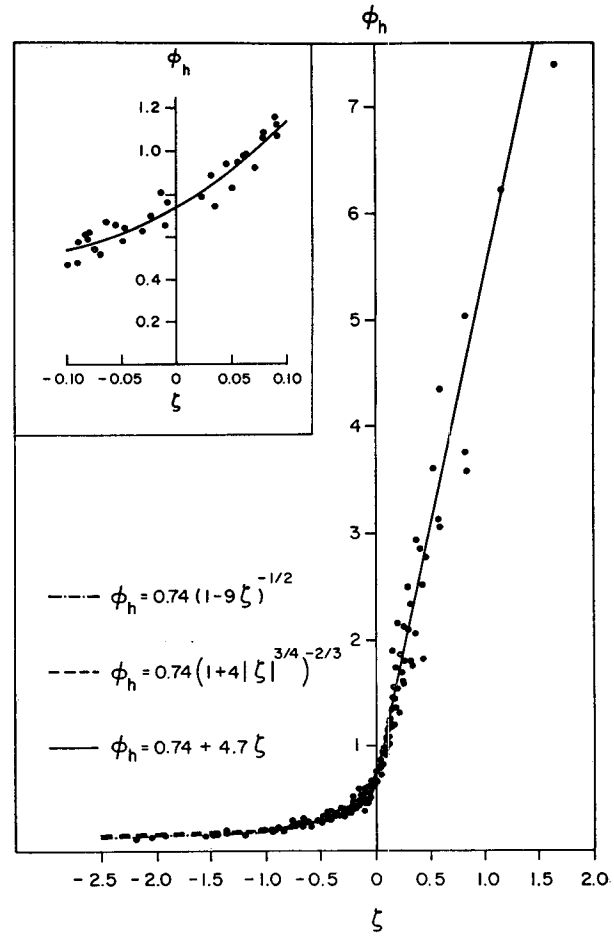

FIG. 2. Comparison of dimensionless temperature gradient observations with interpolation formulas.

cated by the observations; apparently the slope of ϕ_m changes rapidly as the neutral point is crossed.

b. Dimensionless temperature gradient, $\phi_h(\zeta)$

A plot of ϕ_h vs ζ is given in Fig. 2. Again we find that the results show remarkably little scatter, thus permitting a careful comparison with existing interpolation formulas.

First we note that $\phi_h(0)$ does not appear to be equal to 1.0, but is $\sim$0.74. This means that the ratio of the eddy diffusivities is not unity even for neutral conditions, a point discussed in more detail later.

The normalized function $\phi_h(\zeta)/\phi_h(0)$ has been compared with the interpolation formulas of Elliott (1966) and of Businger-Dyer (Businger, 1966), respectively, as follows:

$$\phi_h(\zeta)/\phi_h(0)=(1+\gamma_3|\zeta|^{\frac{1}{2}})^{-\frac{2}{3}}, \tag{11}$$

$$\phi_h(\zeta)/\phi_h(0)=(1-\gamma_4\zeta)^{-\frac{1}{2}}, \tag{12}$$

both of which are applicable to unstable conditions.

These functions are very similar to each other and agree rather well with the observations if $\gamma_3=4$ and $\gamma_4=9$, which were obtained with the previously mentioned minimum square error technique. The behavior of ϕ_h near the neutral point has also been investigated by fitting a quadratic curve through the near neutral data, as shown in the inset in Fig. 2. In this case the curve is given by

$$\phi_h=0.74+3.0\zeta+9.2\zeta^2. \tag{13}$$

The slope at the origin is 3.0, in good agreement with the value of 3.3 obtained from the Businger-Dyer formula [Eq. (12)]. Elliott's formula implies an infinite slope at $\zeta=0$ and is not meant to be valid there. A comparison with the corresponding expression for ϕ_m in Eq. (9) shows that the shapes of ϕ_h and ϕ_m are very similar in near-neutral conditions.

In the stable range, ϕ_h is well represented by a linear function of ζ. The curve in Fig. 2 is

$$\phi_h=0.74+4.7\zeta, \tag{14}$$

with an uncertainty of perhaps $\pm$0.5 in the slope due to scatter of the points. As with ϕ_m, we note that the slope changes rapidly from neutral to stable conditions.

The very unstable cases have been plotted separately in Fig. 3 in log-log coordinates to investigate the behavior when approaching free convection. It is evident from this plot that ϕ_h approaches $\zeta^{-\frac{1}{3}}$ behavior rather than the $\zeta^{-\frac{1}{2}}$ predicted originally by Prandtl (1932) and later by Obukhov (1946) and also by Priestley (1954). This is in agreement with Dyer's (1965) analysis of the Kerang and Hay data, and with Eqs. (11) and (12).

As pointed out by Elliott (1966), the observed power law behavior

$$\phi_h\propto\zeta^{-\frac{1}{2}} \tag{15}$$

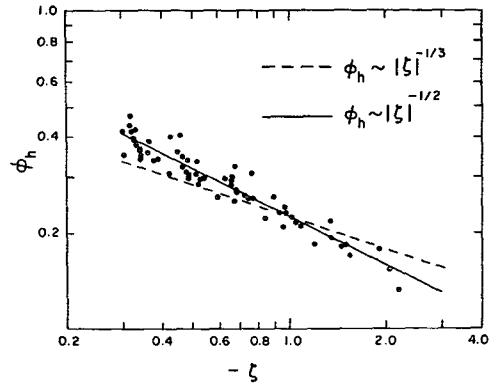

FIG. 3. The dimensionless temperature gradient under very unstable conditions.

implies, from the definitions of ϕ_h and ζ, that

$$\frac{\partial\bar{\theta}}{\partial z}\approx(\overline{w'\theta'})^{\frac{1}{2}}\left(\frac{g}{\bar{\theta}}\right)^{-\frac{1}{2}}u_*^{\frac{1}{2}}z^{-\frac{3}{2}}. \tag{16}$$

On the other hand, the result

$$\phi_h\propto\zeta^{-\frac{1}{3}} \tag{17}$$

is based on the assumption that u_* no longer enters as a basic variable, so that

$$\frac{\partial\bar{\theta}}{\partial z}\approx(\overline{w'\theta'})^{\frac{1}{2}}\left(\frac{g}{\bar{\theta}}\right)^{-\frac{1}{3}}z^{-\frac{1}{3}}. \tag{18}$$

If the observed behavior continues to the true free convection state, where u_* vanishes, we have a dilemma, since Eq. (16) indicates that the temperature gradient then vanishes as well. In the atmosphere, the temperature gradient usually vanishes at 100 m or so under unstable conditions, and there is a tendency for this height to decrease with increasing instability, as can be deduced from the Cedar Hill observations (Kaimal, 1966). Nevertheless, $\partial\bar{\theta}/\partial z$ cannot vanish near the surface. Therefore, if Eq. (16) describes the correct height dependence for conditions approaching and including free convection, a new scale has to be introduced to replace u_*. This implies, contrary to the assumption leading to Eq. (18), that the independent parameters $\overline{\theta'w'}$, z and $g/\bar{\theta}$ are not sufficient to determine the temperature gradient. Perhaps the additional scale needed is a velocity scale characteristic of the large convective eddies. Free convection observations in the atmosphere are very scarce, however, and the verification of this speculation will have to wait for better documentation of free convection.

c. Ratio of eddy diffusivities

In a constant stress layer, the definition of α,

$$\alpha=\frac{K_h}{K_m}=\frac{\overline{w'\theta'}}{\overline{u'w'}}\frac{\partial\bar{U}/\partial z}{\partial\bar{\theta}/\partial z}, \tag{19}$$

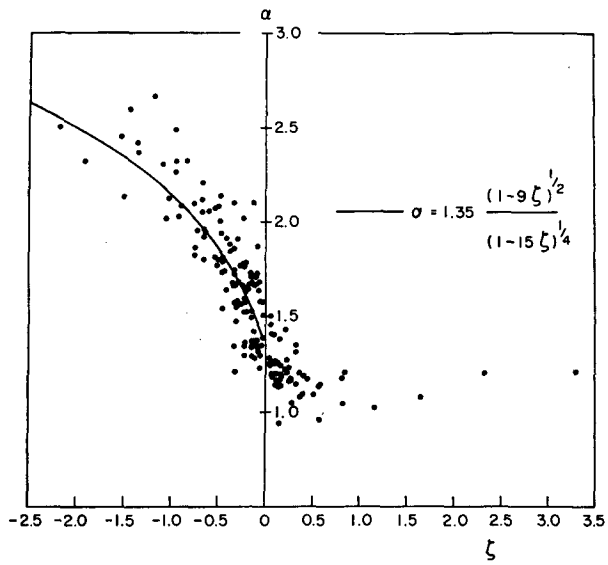

FIG. 4. The dependence of the ratio of eddy diffusivities on stability.

can be rewritten by replacing $\overline{u'w'}$ with $-u_*^2$, with the result

$$\alpha=\frac{\phi_m}{\phi_h}. \tag{20}$$

Values of α found from Eq. (20) are shown in Fig. 4. The scatter is significantly greater than in the ϕ_m and ϕ_h plots, because u_* is the chief source of the scatter, and the effect on α is greater since it contains u_*^2. Nevertheless, it is clear that α increases with increasing instability. It also appears, as we remarked earlier, that in neutral conditions α is $\sim$1.35, and not 1.0 as has been suggested in the past. This value of 1.35 is in close agreement with laboratory measurement (cf. Hinze, 1959).

Much of the previous work on α has been carried out without the benefit of direct stress measurements. Some insight into the difficulty imposed by this approach can

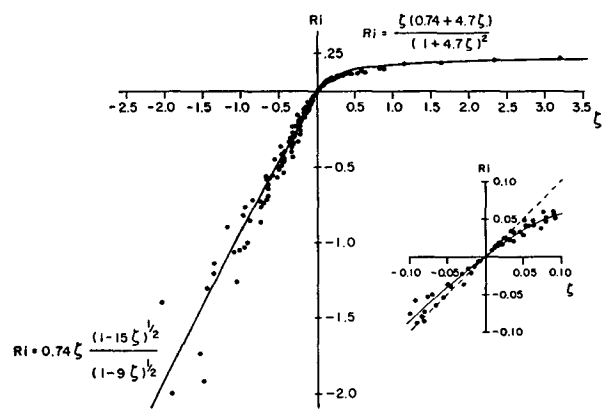

FIG. 5. The dependence of Richardson number on stability.

be gained by rewriting Eq. (19) as

$$\alpha=\frac{\overline{w'\theta'}}{-u_*^2}\frac{\partial\bar{U}/\partial z}{\partial\bar{\theta}/\partial z}. \tag{21}$$

In the absence of direct measurements, u_* can be inferred from wind profiles. At neutrality, the profile is simply

$$\bar{U}=\frac{u_*}{k}\ln\left(\frac{z}{z_0}\right). \tag{22}$$

The roughness length z_0 is found by extrapolating the profile to zero speed; knowing k, u_* can then be found from Eq. (22). The important point here is that the use of the usual value of 0.40 for k would lead to u_* values about 15% high, in view of our finding that $k=0.35$. Use of these high u_* values in Eq. (21) then would give low values for α; a true value of $\alpha=1.35$ would decrease to about 1.0. It is probable that this accounts for the difference between our α value and some of the lower values in the literature.

For the unstable range, the Businger-Dyer equations (8) and (12) in Eq. (20) give

$$\alpha=\frac{1.35(1-9\zeta)^{\frac{1}{2}}}{(1-15\zeta)^{\frac{1}{4}}}. \tag{23}$$

Eq. (23) has been plotted in Fig. 4. The fit is as good as the scattered data would allow. The KEYPS description assumes $\alpha=1.0$ and therefore does not give a basis for comparison,

The data do not appear to indicate a specific trend in the stable range. From Eqs. (10) and (14), however, we can write

$$\alpha=\frac{1.0+4.7\zeta}{0.74+4.7\zeta}, \tag{24}$$

which indicates that α decreases slowly with increasing ζ under stable conditions, asymptotically approaching 1.0. The α data (Fig. 4) show too much scatter for a critical test of Eq. (24), but it does appear that α is roughly constant, with a value between 1.0 and 1.35. In this stable regime, the scatter is reduced considerably if α is calculated from the local measured values of heat flux and stress. In this case it is found that α decreases very slowly with increasing stability, much as predicted by Eq. (24), with an average value for the stable observations of $\sim$1.2.

d. The function Ri(ζ)

Knowledge of the relationship between Ri and ζ is obviously of value in studying data which include no direct flux measurements, and hence no ζ values. We can derive an expression which fits our data well by starting with the relation

$$\zeta=\alpha\phi_m\mathrm{Ri}. \tag{25}$$

Under unstable conditions, the Businger-Dyer formulas were found to fit the observations well, and led to the expressions for ϕ_m and α, given in Eqs. (8) and (23), respectively; these together with Eq. (25) give

$$\mathrm{Ri}=\frac{0.74\zeta(1-15\zeta)^{\frac{1}{2}}}{(1-9\zeta)^{\frac{1}{2}}}. \tag{26}$$

Eq. (26) fits well, as shown in Fig. 5.

It has been suggested independently by Pandolfo (1966), Businger (1966), and Dyer (unpublished) that $\mathrm{Ri}=\zeta$ is a good practical approximation. Very close to neutral, we can write

$$\mathrm{Ri}\approx\left(\frac{\partial \mathrm{Ri}}{\partial\zeta}\right)_0\zeta=\phi_h(0)\zeta=0.74\zeta, \tag{27}$$

so that here the approximation $\mathrm{Ri}=\zeta$ is only fair, as shown in the inset in Fig. 5. At $\zeta=-0.1$, however, the deviation between $\mathrm{Ri}=\zeta$ and Eq. (26) is only 15%, and it decreases asymptotically to about 4% as $\zeta\to-\infty$. The simple expression $\mathrm{Ri}=\zeta$ is therefore a good overall approximation for unstable conditions.

Under stable conditions, Eqs. (10), (24) and (25) imply that

$$\mathrm{Ri}=\frac{\zeta(0.74+4.7\zeta)}{(1+4.7\zeta)^2}, \tag{28}$$

which, as shown in Fig. 5, fits the data very well. Wind tunnel observations of this relation, by Arya and Plate (1969), although extending over a smaller stability range, show the same behavior. Eq. (28) shows that Ri approaches a limit of 0.21 as $\zeta\to\infty$. In an analogous way, Webb (1970) obtained a limit of about 0.20. If, as conditions become more stable, the heat flux and Reynolds stress approach zero at the same rate, then L approaches zero because it contains these terms to different powers. Then $\zeta\to\infty$ as the turbulence diminishes and the flow becomes laminar, and we can interpret the limiting value of Ri as the critical Richardson number. It should be emphasized that our value of 0.21 was obtained from a limited amount of data and more observations are needed for substantiation.

e. *Flux computations from profiles*

Since both ϕ_m and ϕ_h are described accurately by interpolation formulas, stress and heat flux estimates obtained by fitting integrals of these formulas to the raw profiles would be expected to agree well with the directly measured values. However, this comparison is useful in giving an indication of the accuracy with which an individual run may yield its fluxes using profile formulas, as shown by the scatter about the one-to-one lines.

By fitting Eqs. (8) and (12) in integrated form to the measured wind and temperature profiles for the unstable range, u_*, θ_*, z_0, and consequently the fluxes as well can be determined. A detailed discussion of this technique has been given by Paulson (1967). Fluxes calculated in this manner from the 15-min profiles have been plotted vs the observed values in Figs. 6 and 7. It is clear that the data scatter around a one-to-one relation as expected.

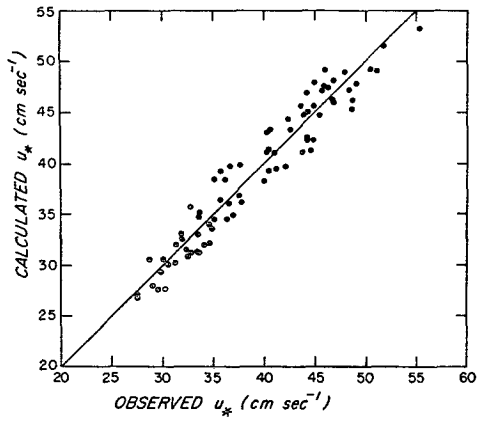

FIG. 6. Comparison of profile-derived and observed friction velocities, unstable cases.

For the stable cases, fluxes were calculated by using the integrated forms of Eqs. (10) and (14), i.e.,

$$\bar{U}=\frac{u_*}{k}\left(\ln\frac{z}{z_0}+4.7\zeta\right), \tag{29}$$

$$\bar{\theta}=\theta_0+\theta_*\left(0.74\ln\frac{z}{z_0}+4.7\zeta\right), \tag{30}$$

with $z_0=2.44$ cm, which was obtained from the analyses of the unstable cases. For each 15-min stable period, except those during transition periods, u_* and L were found by minimizing the mean square error between the observations and Eq. (29). The calculated values of

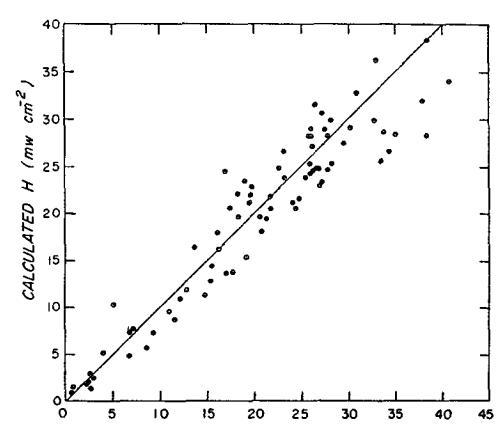

FIG. 7. Comparison of profile-derived and observed heat fluxes, unstable cases.

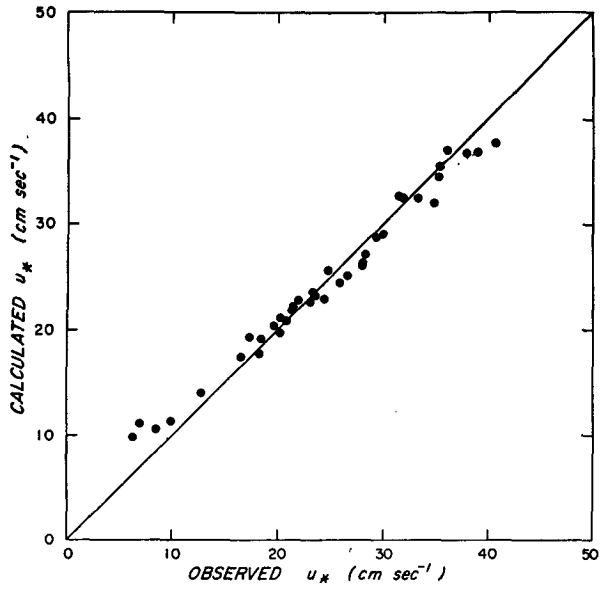

FIG. 8. Comparison of profile-derived and observed friction velocities, stable cases.

u_* are plotted against the observed values in Fig. 8, and it is obvious that the agreement is good.

The heat flux was found similarly. Values of θ_* and θ_0 were found by minimizing the mean square error between Eq. (30) and each 15-min temperature profile, using L values found during the u_* calculation. From the definition of θ_*, the heat flux was then obtained by using the profile-derived u_*. The heat fluxes calculated in this manner are compared with the observed heat fluxes in Fig. 9. The agreement is not as good as found for the unstable cases (Fig. 7). It should be mentioned that in both Figs. 8 and 9 the data points with the smallest values of u_* and heat flux were those with Richardson numbers close to the critical value.

An independent set of observations will be required to test the validity of these results, since the free constants in the profile formulas were determined by optimizing the fit to the data. The relatively small scatter does indicate, however, that the profile technique can be a simple and useful means of obtaining the fluxes.

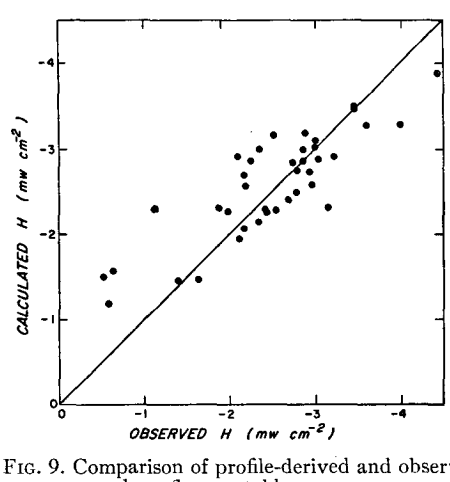

FIG. 9. Comparison of profile-derived and observed heat fluxes, stable cases.

5. Conclusions

The following conclusions appear warranted by the analyses described above:

1) The predictions of the similarity theory of Monin and Obukhov are well satisfied by the data.

2) The wind shear data indicate that von Kármán's constant is ~0.35 rather than the widely used value of 0.40.

3) The ratio of the eddy diffusivities for heat and momentum is greater than unity. The value at neutral is 1.35; it decreases slightly in stable conditions, and shows a marked increase with instability.

4) The relationship between Ri and ζ shows remarkably small scatter, and is nearly linear in unstable conditions; on the stable side, Ri approaches a limit of about 0.21 as $\zeta \to \infty$.

5) Profile-derived and measured fluxes agree well over the entire stability range of the observations, but an independent set of observations is needed to verify this conclusion.

Acknowledgments. The authors wish to acknowledge the joint effort of all members of the Boundary Layer Branch of AFCRL, who planned and carried out the 1968 Kansas field trip which supplied the data for this paper. Particular thanks are due to Dr. D. A. Haugen for his critical review of the manuscript, to Mr. R. Sizer for preparing the drawings, and to Miss S. Tourville for typing the manuscript.

REFERENCES

Arya, S. P. S., and E. J. Plate, 1969: Modeling of the stably stratified atmospheric boundary layer. *J. Atmos. Sci.*, **26**, 656–665.

Bradley, E. F., 1968: A shearing stress meter for micrometeorological studies. *Quart. J. Roy. Meteor. Soc.*, **94**, 380–387.

——, 1969: A small sensitive anemometer system for agricultural meteorology. *Agric. Meteor.*, **6**, 185–193.

Businger, J. A., 1966: Transfer of heat and momentum in the atmospheric boundary layer. *Proc. Arctic Heat Budget and Atmospheric Circulation*. Santa Monica, Calif., RAND Corp., 305–332.

Charnock, H., 1967: Flux gradient relations near the ground in unstable conditions. *Quart. J. Roy. Meteor. Soc.*, **93**, 97–100.

Dyer, A. J., 1965: The flux-gradient relation for turbulent heat transfer in the lower atmosphere. *Quart. J. Roy. Meteor. Soc.*, **91**, 151–157.

——, 1967: The turbulent transport of heat and water vapour in an unstable atmosphere. *Quart. J. Roy. Meteor. Soc.*, **93**, 501–508.

——, 1968: An evaluation of eddy flux variation in the atmospheric boundary layer. *J. Appl. Meteor.*, **7**, 845–850.

Elliott, W. P., 1966: Daytime temperature profiles. *J. Atmos. Sci.*, **23**, 678–681.

Frenzen, Paul, 1966: On some limitations to the use of cup anemometers in micrometeorological measurement. Ann. Rept., Argonne Natl. Lab., Radiological Phys. Div., 100–103.

Haugen, D. A., J. C. Kaimal and E. F. Bradley, 1971: An experimental study of Reynolds stress and heat flux in the atmospheric surface layer. *Quart. J. Roy. Meteor. Soc.* (in press).

Hinze, J. O., 1959: *Turbulence.* New York, McGraw-Hill, 586 pp.

Izumi, Y., and M. L. Barad, 1970: Wind speeds as measured by cup and sonic anemometers and influenced by tower structure. *J. Appl. Meteor.*, **9**, 851–856.

Kaimal, J. C., 1966: An analysis of sonic anemometer measurements from the Cedar Hill tower. Environmental Res. Paper No. 215, AFCRL-66-542.

——, and J. T. Newman, 1966: A computer-controlled mobile micrometeorological observation system. *J. Appl. Meteor.*, **5**, 411–420.

——, and D. A. Haugen, 1969: Some errors in the measurement of Reynolds stress. *J. Appl. Meteor.*, **8**, 460–462.

Lumley, J. L., and H. A. Panofsky, 1964: *The Structure of Atmospheric Turbulence.* New York, Interscience, 239 pp.

MacCready, P. B., Jr., 1966: Mean wind speed measurements in turbulence. *J. Appl. Meteor.*, **5**, 219–225.

Monin, A. S., and A. M. Obukhov, 1954: Basic laws of turbulent mixing in the ground layer of the atmosphere. *Akad. Nauk SSSR Geofiz. Inst. Tr.*, **151**, 163–187.

Obukhov, A. M., 1946: Turbulence in an atmosphere with inhomogeneous temperature. *Tr. Inst. Teor. Geofiz. Akad. Nauk SSSR*, **1**, 95–115.

Pandolfo, J. P., 1966: Wind and temperature for constant flux boundary layers in lapse conditions with a variable eddy conductivity to eddy viscosity ratio. *J. Atmos. Sci.*, **23**, 495–502.

Panofsky, H. A., 1963: Determination of stress from wind and temperature measurements. *Quart. J. Roy. Meteor. Soc.*, **89**, 85–94.

Paulson, C. A., 1967: Profiles of wind speed, temperature, and humidity over the sea. Ph.D. thesis and Sci. Rept., Dept. of Atmos. Sci., University of Washington, Seattle.

Prandtl, L., 1932: Meteorologische Anwendungen der Stromungslehre. *Beitr. Phys. Atmos.*, **19**, 188–202.

Priestley, C. H. B., 1954: Convection from a large horizontal surface. *Australian J. Phys.*, **6**, 279–290.

Stevens, D. W., 1967: High-resolution measurement of air temperature and temperature differences. *J. Appl. Meteor.*, **6**, 179–185.

Swinbank, W. C., 1964: The exponential wind profile. *Quart. J. Roy. Meteor. Soc.*, **90**, 119–135.

——, 1968: A comparison between predictions of dimensional analysis for the constant-flux layer and observations in unstable conditions. *Quart. J. Roy. Meteor. Soc.*, **94**, 460–467.

——, and A. J. Dyer, 1968: Micrometeorological expeditions, 1962–1964. Tech. Paper No. 17, Div. of Meteor. Phys., CSIRO, Australia.

Tennekes, H., 1968: Outline of a second-order theory of turbulent pipe flow. *AIAA Journal*, **6**, 1735–1740.

Webb, E. K., 1970: Profile relationships: The log-linear range and extension to strong stability. *Quart. J. Roy. Meteor. Soc.*, **96**, 67–90.